

Beltrami Signature: A Novel Invariant 2D Shape Representation for Object Classification

Chenran Lin Lok Ming Lui

Abstract

There is a growing interest in shape analysis in recent years and in this paper we present a novel contour-based shape representation named Beltrami signature for 2D bounded simple connected domain. The proposed representation is based on conformal welding. With suitable normalization, the uniqueness of welding is guaranteed up to a rotation. Then it can be extended to a harmonic function and finally quasi-conformal theory get rid of the only uncertainty by computing Beltrami coefficient of harmonic extension. The benefits of the proposed signature is it keeps invariant under simple transformations like scaling, transformation and rotation and is robust under slight deformation and distortion. Experiments demonstrates the above properties and also shows the excellent classification performance.

Index terms—Shape representation, conformal welding, simple connected,invariance

1 Introduction

The outline of the shape contains very important information and it can be used in many applications, such as segmentation, recognition, registration and so on. However, even for the simplest situation, 2D simple connected shapes, it is a big challenge to describe clearly what the shape contour looks like. Because of the complexity of the image, there is an urgent demand to find a common, simple and robust shape representation for further mining and utilizing of shapes' geometric information. Therefore, many different presentations and measures have been widely studied and proposed recently [1, 2, 3, 4, 5, 6, 7].

Considering 2D simple connected shapes, conformal welding is a kind of well-known shape signature. Given 2D simple connected domain $\Omega \subset \mathbb{C}$ with Jordan curve boundary $\eta = \partial\mathbb{D}$, there exist conformal function $\Phi_1 : \mathbb{D} \rightarrow \Omega$ and $\Phi_2 : \mathbb{D}^c \rightarrow \Omega^c$, then conformal welding can be defined as $f = \Phi_1^{-1} \circ \Phi_2$. This gives a simple but wonderful representation of Ω as Fig. 1 shows. However, it has two fatal defects. First is that such representation is not unique. Because of the arbitrary of Riemann conformal mapping, Φ_1 and Φ_2 can only be determined up to a Möbius transformation, so such conformal welding is not unique. Generally speaking, some assumption is required to remove this uncertainty. For example, Sharon *et al.* [8] need to select a base point P inside the given domain Ω artificially, then let Φ_1 maps 0 to this point P . The work of McTeague *et al.* [9] is based on Schramm-Loewner evolution(SLE) on random surfaces called Liouville quantum gravity, they proved the equivalence

between uniqueness of conformal welding and conformal removable and conculded that if the boundary curve η is an SLE_k for $k \in (0, 4)$ and satisfies some other requirements, the corresponding conformal welding is unique. Some may not that care the uniqueness itself, they used equivalent class to guarantee uniqueness in a broader sense or evne just ignored it [10, 11, 12, 13].

Another thing is that even the conformal welding is very easy to be changed by simple transformations like rotation, scaling and translation. Such a unstable representation is hard to apply in practical applications since these transformations are inevitable in the real world.

The contribution of this paper is that we propose a brand new presentation for 2D simple connected shape based on conformal welding with help of quasi-conformal theorem, which is invariant under simple transformation, and we name it Beltrami signature. Given a shape Ω , $\Phi_1 : \mathbb{D} \rightarrow \Omega$ and $\Phi_2 : \mathbb{D}^c \rightarrow \Omega^c$ can be calculated by zipper algorithm, which is a mature and efficient algorithm to find the conformal mapping from the given domain to unit disk by finite boundary points. Under suitable normalization, conformal welding $f : \partial\mathbb{D} \rightarrow \partial\mathbb{D}$ can be determined up to a rotation. Such conformal welding can be extended to the whole unit disk and get a harmonic function $F : \mathbb{D} \rightarrow \mathbb{D}$ and the Beltrami coefficient of F is our Beltrami signature.

The proposed shape representation, Beltrami signature, is uniquely determined by the given domain without any assumption and artificial restriction to domain. The Beltrami signature is based on computational quasiconformal geometry. Computational quasiconformal geometry has been widely used in image processing and image analysis. Applications can be found in image segmentation [14, 15, 16], image registration [17, 18, 19, 20, 21, 22, 23, 24, 25, 26, 27, 28, 29] and image analysis [30, 31, 32, 33, 34, 35, 36]. What's more worth mentioning is that Beltrami signature is invariant under rotation, translation and scaling and is robust to small deformation and distortion of the original shape. It means the proposed representation has high practical value and can be applied in computer vision work like classification, segementation and so on.

The paper is organized as follows: Section 2 introduces some theoretic background; Section 3 shows the main theorem and how Beltrami signature is obtained from given domain; Section 4 gives the details about the implementation; Section 5 reports our experimental results. The paper is concluded in Section 6 and we point out future directions.

2 Theoretical basis

2.1 Quasi-conformal mapping and Beltrami equation

Let $f : \Omega \subset \mathbb{C} \rightarrow \mathbb{C}$ be a complex function. The following differential operators are more convenient for discussion

$$\frac{\partial}{\partial z} := \frac{1}{2} \left(\frac{\partial}{\partial x} - i \frac{\partial}{\partial y} \right), \quad \frac{\partial}{\partial \bar{z}} := \frac{1}{2} \left(\frac{\partial}{\partial x} + i \frac{\partial}{\partial y} \right)$$

f is said to be *quasi-conformal* associated to μ if it orientation-preserving and satisfies the following *Beltrami equation*:

$$\frac{\partial f}{\partial \bar{z}} = \mu(z) \frac{\partial f}{\partial z} \tag{1}$$

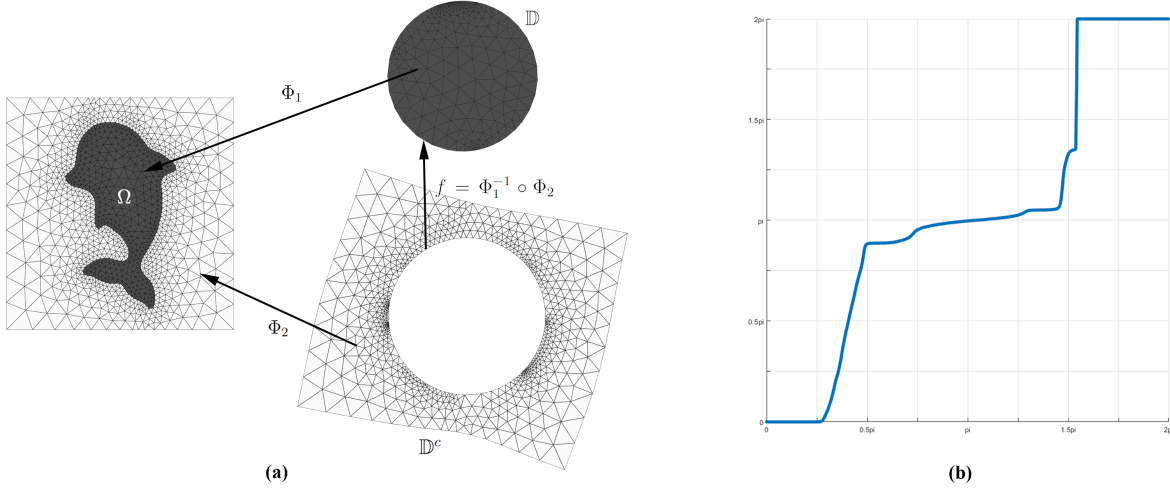


Figure 1: (a) The Illustration of how conformal welding f is defined from given 2D simple connected domain Ω . (b) The image of conformal welding $f : [0, 2\pi) \rightarrow [0, 2\pi)$

where $\mu(z)$ is some complex-valued Lebesgue measurable function satisfying $\|\mu\|_\infty < 1$. More specifically, this $\mu : \Omega \rightarrow \mathbb{D}$ is called the *Beltrami coefficient* of f

$$\mu = \frac{f_{\bar{z}}}{f_z} \quad (2)$$

In terms of the metric tensor, consider the effect of the pullback under f of the Euclidean metric ds_E^2 ; the resulting metric is given by:

$$f^*(ds_E^2) = \left| \frac{\partial f}{\partial z} \right|^2 |dz + \mu(z)d\bar{z}|^2 \quad (3)$$

which, relative to the background Euclidean metric dz and $d\bar{z}$, has eigenvalue $(1 + |\mu|)^2 \left| \frac{\partial f}{\partial z} \right|^2$ and $(1 - |\mu|)^2 \left| \frac{\partial f}{\partial z} \right|^2$. μ is called the *Beltrami coefficient*, which is a measure of nonconformality. In particular, the map f is conformal around a small neighborhood of p when $\mu(p) = 0$. Infinitesimally, around a point p , f may be expressed with respect to its local parameters as follows:

$$f(z) = f(p) + f_z(p)z + f_{\bar{z}}(p)\bar{z} = f(p) + f_z(p)(z + \mu(p)\bar{z}). \quad (4)$$

If $\mu(z) = 0$ everywhere, then f is called *conformal* or *holomorphic*. A conformal map satisfies the following well-known Cauchy-Riemann equation:

$$\frac{\partial f}{\partial \bar{z}} = 0. \quad (5)$$

Inside the local parameter domain, f may be considered as a map composed of a translation to $f(p)$ together with a stretch map $S(z) = z + \mu(p)\bar{z}$, which is postcomposed by multiplication of $f_z(p)$, which is conformal. All the conformal distortion of $S(z)$ is caused by $\mu(p)$.

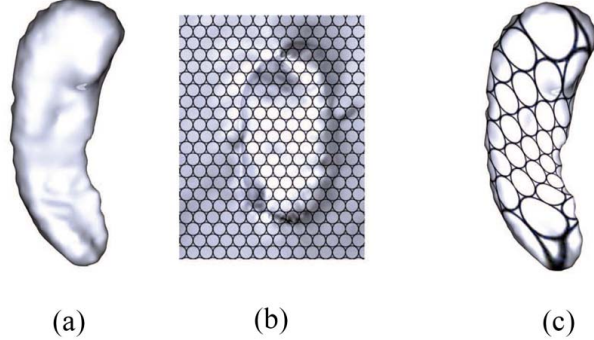


Figure 2: (a) Shows the original hippocampus. (b) Shows the parameter domain with circle packing pattern. Under the quasiconformal parameterization, the infinitesimal circles on the parameter domain are mapped to infinitesimal ellipses on the hippocampus, as shown in (c).

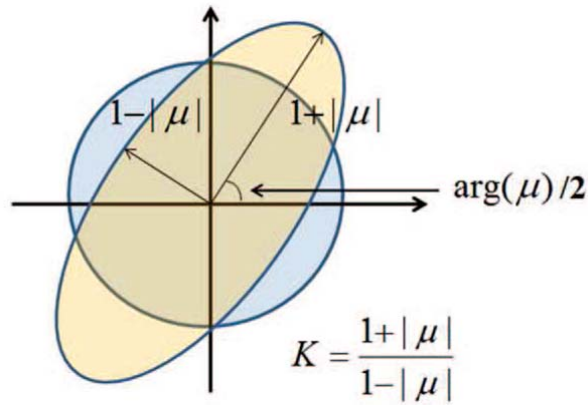


Figure 3: Quasi-conformal maps infinitesimal circles to ellipses. The Beltrami coefficient measure the distortion or dilation of the ellipse under the QC map.

$S(z)$ is the map that causes f to map a small circle to a small ellipse (see Fig. 2). Form $\mu(p)$, we can determine the angles of the directions of maximal magnification and shrinkage and the amount of them as well. Specially, the angle of maximal magnification is $\arg(\mu(p))/2$ with magnifying factor $1 + |\mu(p)|$; the angle of maximal shrinkage is the orthogonal angle $\arg(\mu(p))/2 - \pi/2$ with shrinkage factor $1 - |\mu(p)|$. The distortion or dilation is given by:

$$K = \frac{1 + |\mu(p)|}{1 - |\mu(p)|}. \quad (6)$$

Thus, the Beltrami coefficient μ gives us important information about the properties of the map (see Fig. 3).

Suppose $f, g : \mathbb{C} \rightarrow \mathbb{C}$ are complex-valued function with Beltrami coefficient μ_f, μ_g respectively. Then the Beltrami coefficient for the composition $g \circ f$ is given by

$$\mu_{g \circ f} = \frac{\mu_f + (\mu_g \circ f)\tau}{1 + \overline{\mu_f}(\mu_g \circ f)\tau}, \quad (7)$$

where $\tau = \frac{\bar{f}_z}{f_z}$. Note that when g is conformal, $\mu_g = 0$ and

$$\mu_{g \circ f} = \mu_f. \quad (8)$$

2.2 Conformal welding

Given 2D bounded simple connected shape, we can treat it as a boundary simple connected domain $\Omega \subset \mathbb{C}$, by Riemann mapping theorem, there exist conformal function $\Phi_1 : \mathbb{D} \rightarrow \Omega$ and $\Phi_2 : \mathbb{D}^c \rightarrow \Omega^c$. Φ_1 and Φ_2 are unique up to a *Mobious transformation*:

$$M(z) = e^{i\theta} \frac{z - a}{1 - \bar{a}z}. \quad (9)$$

Then we can define *conformal welding* as:

$$f = \Phi_1^{-1} \circ \Phi_2. \quad (10)$$

Such $f : \partial\mathbb{D} \rightarrow \partial\mathbb{D}$ is a diffeomorphism from $\partial\mathbb{D}$ to itself, which can be also thought as a periodic, real-valued monotone increasing function $f_{\mathbb{R}} : [0, 2\pi) \rightarrow [0, 2\pi)$ such that $f(e^{i\theta}) = e^{if_{\mathbb{R}}(\theta)}$ (see Fig. 1).

2.3 Harmonic function and Poisson integral

A complex-valued function f defined on $\Omega \subset \mathbb{C}$ is called *harmonic* if it satisfies the *Laplace's equation*:

$$\Delta f = 4 \frac{\partial^2 f}{\partial z \partial \bar{z}} = \frac{\partial^2 f}{\partial x^2} + \frac{\partial^2 f}{\partial y^2} = 0, \quad (11)$$

where $z = x + iy$, x, y is the real and imaginary value.

Chen *et al.* prove following theorem in [37], which tells us that the composition of harmonic mappings and other mappings can inherit such harmonicity in some condition.

Theorem 1. *Let f be a harmonic mapping, $f \circ g$ is harmonic if and only if $g(z) = az + b\bar{z} + c$, where a, b and c are constants and $g \circ f$ is harmonic if and only if g is analytic or anti-analytic.*

The harmonic function on a compact set is determined by its restriction to the boundary, which follows from the maximum principle, and the progress of find a harmonic function from the given domain and continuous boundary value is call *Dirichlet problem*. For a special case, where the domain is unit disk on complex plane, *Poisson integral* shows a method to obtain the solution $F : \overline{\mathbb{D}} \rightarrow \mathbb{C}$ of Dirichlet problem from a continuous f on $\partial\mathbb{D}$

$$F(re^{i\theta}) = \frac{1}{2\pi} \int_0^{2\pi} \frac{(1 - r^2)f(e^{i\varphi})}{1 - 2rcos(\varphi - \theta) + r^2} d\varphi. \quad (12)$$

Such F is harmonic on \mathbb{D} and continuous on $\overline{\mathbb{D}}$ and have the same value with f on the $\partial\mathbb{D}$, i.e. $F(e^{i\theta}) = f(e^{i\theta})$ (see Fig. 4). Of course, this F is unique.

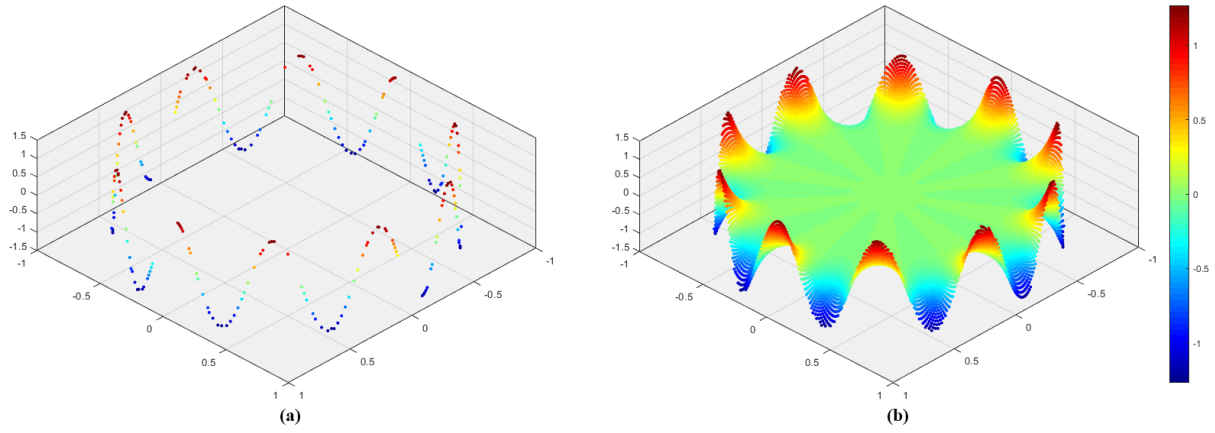


Figure 4: (a) Continuous function $f(e^{i\theta}) = \sin(100\theta) + \cos(100\theta)$ defined on $\partial\mathbb{D}$. (b) The corresponding harmonic function F generated from f by the equation (12). Note that we used real-valued function to illustrate the progress of harmonic extension for the convenience of demonstration.

3 Beltrami signature

In this chapter, we will propose a new signature, Beltrami signature, to represent boundary simple connected domain Ω . Our proposed signature is based on conformal welding. But with some normalization.

3.1 Beltrami signature based on conformal welding

Here we give a brief explanation of how to create our new signature. Given the boundary simple connected domain $\Omega \subset \mathbb{C}$, we can get conformal welding $f = \Phi_1^{-1} \circ \Phi_2$ of it. Note that with some suitable normalization methods, which will be revealed in detail in Section 3.3 and 3.4, f is determined up to a rotation. Then f can be extended to harmonic function F defined on \mathbb{D} by Poisson integral. At the end, the Beltrami coefficient of F becomes a signature of domain Ω , we call it as *Beltrami signature*:

$$B := \mu_F = \frac{F_{\bar{z}}}{F_z}. \quad (13)$$

3.2 Analysis of uniqueness of Beltrami signature

According to Riemann mapping theorem, the conformal mapings $\Phi_1 : \mathbb{D} \rightarrow \Omega$ and $\Phi_2 : \mathbb{D}^c \rightarrow \Omega^c$ are not unique. Suppose $\tilde{\Phi}_1 : \mathbb{D} \rightarrow \Omega$, $\tilde{\Phi}_2 : \mathbb{D}^c \rightarrow \Omega^c$ are also conformal and $\tilde{\Phi}_1 = \Phi_1 \circ M_1$, $\tilde{\Phi}_2 = \Phi_2 \circ M_2$, where M_1, M_2 are Möbius transformations. Therefore, the corresponding conformal welding is

$$\tilde{f} = \tilde{\Phi}_1^{-1} \circ \tilde{\Phi}_2 = M_1^{-1} \circ \Phi_1^{-1} \circ \Phi_2 \circ M_2 = M_1^{-1} \circ f \circ M_2. \quad (14)$$

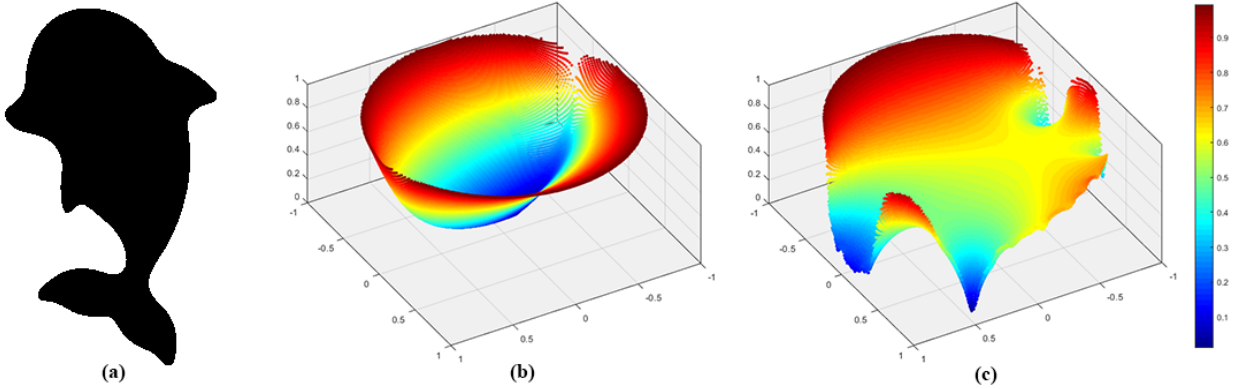


Figure 5: Illustration of Beltrami signature. (a) The input shape, a dolphin. (b) The corresponding harmonic extension, where the conformal welding is shown in Fig 1 (b). (c) The Beltrami signature of original shape. Remark that the harmonic function and Beltrami signature should be complex-valued function and we only show modulus of them in z-axis in (b) and (c).

With equation (12), it can be also extended to harmonic function \tilde{F} . The following theorem show the relationship between F and \tilde{F} .

Theorem 2. Suppose f and \tilde{f} are continuous map from $\partial\mathbb{D}$ to itself and $\tilde{f} = M_1^{-1} \circ f \circ M_2$, where M_1, M_2 are both Möbius transformations. F and \tilde{F} are harmonic extension of f and \tilde{f} , then $\tilde{F} = M_1^{-1} \circ F \circ M_2$ iff M_1 is a rotation.

Proof. Since M_1 is a Möbius transformations, M_1^{-1} is also a Möbius transformation, so it can be written as $M_1^{-1}(z) = e^{i\theta} \frac{z-p}{1-\bar{p}z}$, where $\theta \in [0, 2\pi)$ and $p \in \mathbb{D}$.

\Rightarrow : When $\tilde{F} = M_1^{-1} \circ F \circ M_2$, from Theorem 1 we can know that $F \circ M_2$ is harmonic since there is no doubt that Möbius transformation M_2 is conformal. \tilde{F} and $F \circ M_2$ are both harmonic, so $M_1^{-1}(z) = az + b\bar{z} + c$, where $a, b, c \in \mathbb{C}$. Therefore, we have

$$e^{i\theta} \frac{z-p}{1-\bar{p}z} = az + b\bar{z} + c,$$

which means $p = b = c = 0$, $a = e^{i\theta}$ and so M_1 is a rotation.

\Leftarrow : When M_1 is a rotation, M_1^{-1} is also a rotation, so $M_1^{-1} \circ F \circ M_2$ is a harmonic function according to Theorem 1. It's easy to check that

$$M_1^{-1} \circ F \circ M_2(e^{i\theta}) = M_1^{-1} \circ f \circ M_2(e^{i\theta}) = \tilde{f}(e^{i\theta}) = \tilde{F}(e^{i\theta}),$$

which means $M_1^{-1} \circ F \circ M_2$ and \tilde{F} have the same boundary value. From the uniqueness of harmonic mapping, $M_1^{-1} \circ F \circ M_2 = \tilde{F}$. \square

Because of above theorem, suppose that M_1 is a rotation, then we consider the Beltrami signature of \tilde{F}

$$\tilde{B} = \mu_{\tilde{F}} = \mu_{M_1^{-1} \circ F \circ M_2} = \mu_{F \circ M_2}. \quad (15)$$

If we want such Beltrami signature is unique, which means $\tilde{B} = \mu_{F \circ M_2} = \mu_F = B$, then we get M_2 is identity. Therefore, we know that the uniqueness of Beltrami signature is equivalent to following restrictions:

1. $\Phi_1 : \mathbb{D} \rightarrow \Omega$ should be determined up to a rotation.
2. $\Phi_2 : \mathbb{D}^c \rightarrow \Omega^c$ should be uniquely determined.

3.3 Normalization to Φ_1

We hope Φ_1 is determined up to a rotation. It is not that hard, for example, we can normalize Φ_1 by restricting $\Phi_1(0) = 0$. But it need a hypothesis that 0 is in Ω , which is equivalent to limiting the position of shape and cannot always hold. Here we want to show a new approach which can determine Φ_1 up to a rotation without any additional assumption.

In actual application, we usually only know finite boundary points z_1, z_2, \dots, z_n of Ω . Denote $p_i = \Phi_1^{-1}(z_i) \in \partial\mathbb{D}$, we claims that Φ_1 can be normalized by restricting the center of p_i to 0.

Theorem 3. *Given $\{z_1, z_2, \dots, z_n\} \subset \partial\Omega$ and $n \geq 3$, if conformal mapping $\Phi_1 : \mathbb{D} \rightarrow \Omega$ satisfies*

$$\sum_{k=1}^n \Phi_1^{-1}(z_k) = 0, \quad (16)$$

then such Φ_1 is unique up to a rotation.

Before proving theorem 3, we can consider following problem. Given boundary points p_i on unit circle, can we find a Mobiobus transformation M satisfies the following equation (17)?

$$\sum_{k=1}^n M(p_k) = \sum_{k=1}^n e^{i\theta} \frac{p_k - a}{1 - \bar{a}p_k} = 0 \quad (17)$$

Without lose of generality, we ignore the rotation of M and let $F_a(z) = \frac{z-a}{1-\bar{a}z}$, where $a \in \mathbb{D}$. So F_a is also a Mobiobus transformation and it's sufficient to find $a \in \mathbb{D}$ such that

$$f(a) = \sum_{k=1}^n F_a(p_k) = \sum_{k=1}^n \frac{p_k - a}{1 - \bar{a}p_k} = 0 \quad (18)$$

to show the equation (17) holds for some M . Intuitively, we believe that there is always a unique solution to this equation (18) (see Fig 6).

3.3.1 The solvability of equation (18)

First thing we want to do is to check whether this equation (18) is always solvable. According to Brouwer fixed point theorem, we have

Theorem 4. *Given $\{p_1, p_2, \dots, p_n\} \subset \partial\mathbb{D}$ and $n \geq 3$, let $F_a(z) = \frac{z-a}{1-\bar{a}z}$, where $a \in \mathbb{D}$. The solution of equation (18) always exists.*

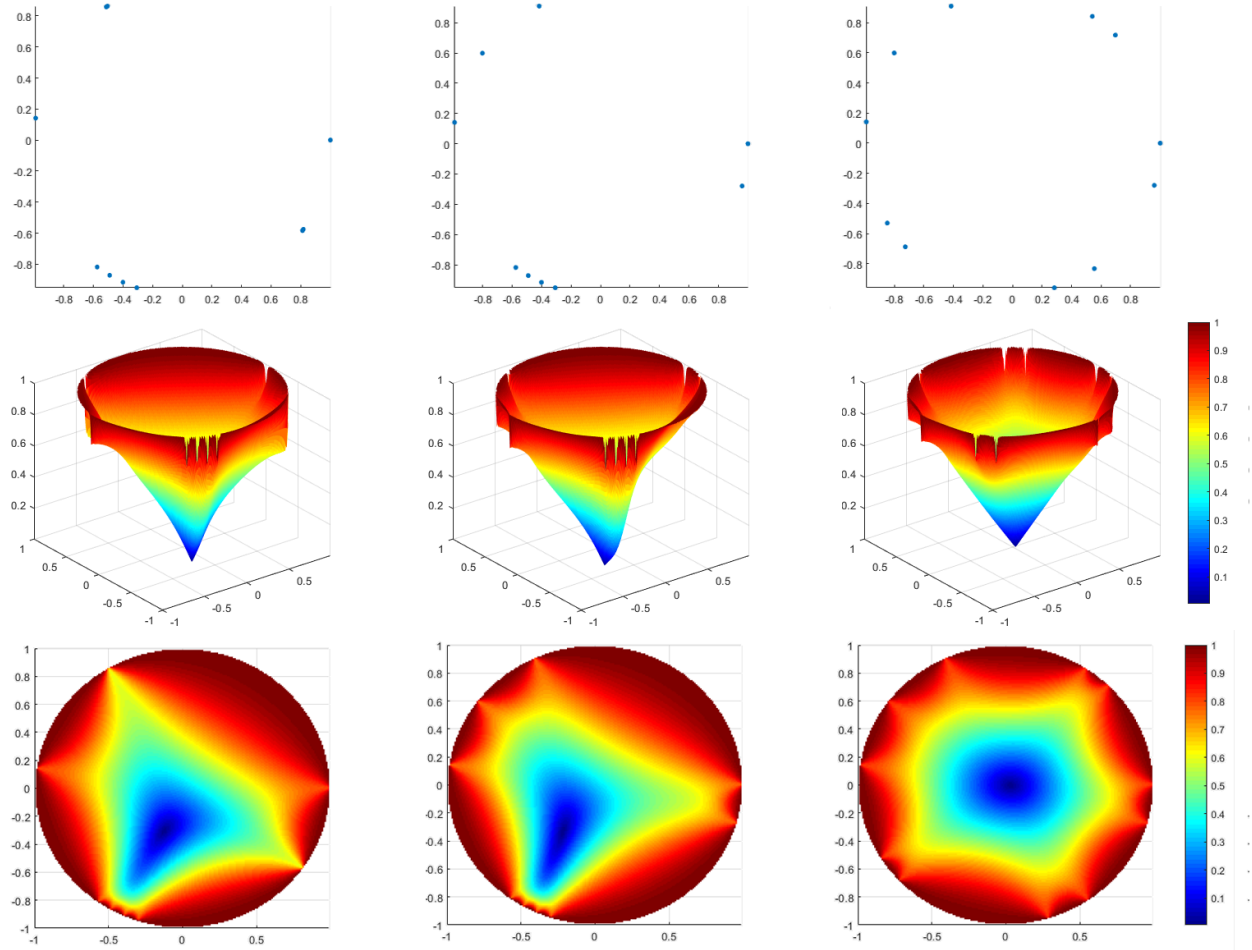


Figure 6: The first row are some randomly generated points in $\partial\mathbb{D}$. The second row are the corresponding $|f(a)|$, where $a \in \mathbb{D}$. The third row are also $|f(a)|$ but is in top view.

Proof. Note that when $e^{i\theta} \neq p_k$ for any k , we have

$$f(e^{i\theta}) = \sum_{k=1}^n \frac{p_k - e^{i\theta}}{1 - e^{-i\theta} p_k} = -ne^{i\theta},$$

so $\frac{1}{n}f(e^{i\theta}) + e^{i\theta} = 0$. Let

$$g(a) = \begin{cases} \frac{1}{n}f(a) + a, & a \in \mathbb{D}, \\ 0, & a \in \partial\mathbb{D}, \end{cases}$$

such g is defined on $\overline{\mathbb{D}}$ and is continuous. It's clear that $\|g(a)\| \leq \frac{1}{n}\|f(a)\| + \|a\| \leq 2$.

Let $M = \{a \in \mathbb{D} \mid \|g(a)\| \geq 1\}$, then define

$$h(a) = \begin{cases} g(a), & a \in \overline{\mathbb{D}} \setminus M, \\ \frac{g(a)}{\|g(a)\|}, & a \in M. \end{cases}$$

h is a continuous map from $\overline{\mathbb{D}}$ to itself, so there exists some a let $h(a) = a$.

If $a \in \partial\mathbb{D}$, $\|a\| = 1$, but $\|h(a)\| = 0 \neq \|a\|$. If $a \in M$, we know $a \notin \partial\mathbb{D}$, so $\|a\| < 1$, but $\|h(a)\| = \frac{\|g(a)\|}{\|g(a)\|} = 1 \neq \|a\|$. So when $h(a) = a$, a is inside $\mathbb{D} \setminus M$. Therefore, such a satisfies $g(a) = a$ and then $f(a) = 0$. \square

Therefore, there must be some $a \in \mathbb{D}$ to be the solution of equation (17).

3.3.2 The uniqueness of the solution of equation (18)

With solvability proved, we naturally want to know if this solution is unique. Let's consider a special case when $\sum_{k=1}^n p_k = 0$, we have

Theorem 5. Suppose $\sum_{k=1}^n p_k = 0$, equation (18) holds if and only if $a = 0$.

Proof. If $a = 0$, it's obvious F_0 is identity, so $f(0) = \sum_{k=1}^n p_k = 0$.

If $a \neq 0$, WLOG, we can assume that $0 < a < 1$, then $F_a(1) = 1$ and $F_a(-1) = -1$. For any $p_k \neq \pm 1$, there is some $\theta_k \in (0, \pi) \cup (\pi, 2\pi)$ such that $p_k = \cos \theta_k + \sin \theta_k i$,

$$F_a(p_k) = F_a(\cos \theta_k + \sin \theta_k i) = \frac{\cos \theta_k + \sin \theta_k i - a}{1 - a \cos \theta_k - a \sin \theta_k i} = \frac{(a^2 + 1) \cos \theta_k - 2a - (a^2 - 1) \sin \theta_k i}{a^2 + 1 - 2a \cos \theta_k},$$

so

$$\operatorname{Re}(F_a(p_k)) = \frac{(a^2 + 1) \cos \theta_k - 2a}{a^2 + 1 - 2a \cos \theta_k} = \cos \theta_k - \frac{2a(1 - \cos^2 \theta_k)}{(a - 1)^2 + 2a(1 - \cos \theta_k)} < \cos \theta_k = \operatorname{Re}(p_k).$$

Therefore, if $n \geq 3$, there must be at least one $p_k \neq \pm 1$ and so

$$\operatorname{Re}\left(\sum_{k=1}^n F_a(p_k)\right) = \sum_{k=1}^n \operatorname{Re}(F_a(p_k)) < \sum_{k=1}^n \operatorname{Re}(p_k) = \operatorname{Re}\left(\sum_{k=1}^n p_k\right) = 0,$$

which means $\sum_{k=1}^n F_a(p_k) \neq 0$. So 0 is the only solution of equation (18) when $\sum_{k=1}^n p_k = 0$. \square

In the fact, no matter how these p_i distribute, we can reduce it to the special mentioned above.

Theorem 6. *The solution of equation (18) is unique.*

Proof. Assume that a_0, a_1 are two different solutions, then we have that

$$\sum_{k=1}^n F_{a_0}(p_k) = 0, \sum_{k=1}^n F_{a_1}(p_k) = 0$$

Let $p'_k = F_{a_0}(p_k)$, then

$$\sum_{k=1}^n F_{a_1} \circ F_{a_0}^{-1} \circ F_{a_0}(p_k) = \sum_{k=1}^n (F_{a_1} \circ F_{-a_0})(F_{a_0}(p_k)) = \frac{1 - a_1 \bar{a}_0}{1 - a_0 \bar{a}_1} \sum_{k=1}^n F_{\frac{a_1 - a_0}{1 - a_1 \bar{a}_0}} p'_k = 0.$$

Since $a_0, a_1 \in \mathbb{D}$, then $\frac{1 - a_1 \bar{a}_0}{1 - a_0 \bar{a}_1} \neq 0$ and so $\sum_{k=1}^n F_{\frac{a_1 - a_0}{1 - a_1 \bar{a}_0}} p'_k = 0$. According to the above claim, $\frac{a_1 - a_0}{1 - a_1 \bar{a}_0} = 0$, so $a_0 = a_1$, which contradicts to the assumption. \square

3.3.3 Unique Φ_1 up to a rotation

Above theorems show that there is alway an unique solution $a \in \mathbb{D}$ of equation (18), so we can come back to theorem (3),

Proof. Suppose Φ_1 and $\tilde{\Phi}_1$ are two arbitrary conformal map from \mathbb{D} to Ω , then $\tilde{\Phi}_1 = \Phi_1 \circ M$, where M is a Mobious transformation. Let $p_k = \Phi_1^{-1}(z_k)$, then we have $\sum_{k=1}^n p_k = 0$ and $\sum_{k=1}^n M^{-1}(p_k) = 0$. M^{-1} is also a Mobious transformation so let $M^{-1}(z) = e^{i\theta} \frac{z-a}{1-\bar{a}z} = e^{i\theta} F_a(z)$, then we have

$$e^{i\theta} \sum_{k=1}^n F_a(p_k) = 0.$$

From theorem 5 we can know $a = 0$, then $M^{-1}(z) = e^{i\theta} z$ and so Φ_1 is unique up to a rotation. \square

3.4 Normalization to Φ_2

As for Φ_2 , we hope it is uniquely determined. Luckily, we always have that $\infty \in \mathbb{D}^c$ and $\infty \in \Omega^c$, then we can use this and derivative to guarantee uniqueness of Φ_2 .

Theorem 7. *If $\Phi_2 : \mathbb{D}^c \rightarrow \Omega^c$ satisfies that*

$$\Phi_2(\infty) = \infty \tag{19}$$

$$1 = \arg \max_{z \in \partial \mathbb{D}} |\Phi_2'(z)|, \tag{20}$$

then such Φ_2 is uniquely determined.

Proof. Φ_2 and $\tilde{\Phi}_2$ are two arbitrary conformal map from \mathbb{D}^c to Ω^c , $\tilde{\Phi}_2 = \Phi_2 \circ M$, where $M(z) = e^{i\theta} \frac{z-a}{1-\bar{a}z}$ is a Mobious transformation. Φ_2 and $\tilde{\Phi}_2$ both satisfy (19), then

$$\tilde{\Phi}_2(\infty) = \Phi_2(M(\infty)) = \infty \text{ and } \Phi_2(\infty) = \infty.$$

Therefore, $M(\infty) = e^{i\theta} \frac{\infty-a}{1-\bar{a}\infty} = \infty$, which means that $a = 0$ and $M(z) = e^{i\theta}z$.

Consider the derivative of $\tilde{\Phi}_2$,

$$\tilde{\Phi}'_2(z) = \Phi'_2 \circ M(z) \cdot M'(z) = e^{i\theta} \Phi'_2(e^{i\theta}z), \quad (21)$$

then we know that $|\tilde{\Phi}'_2(z)| = |\Phi'_2(e^{i\theta}z)|$. Suppose $a = \arg \min_{z \in \partial\mathbb{D}} |\Phi'_2(z)|$ and $ae^{-i\theta} = \arg \min_{z \in \partial\mathbb{D}} |\tilde{\Phi}'_2(z)|$. If condition (20) holds for both Φ_2 and $\tilde{\Phi}_2$, then $a = ae^{-i\theta} = 1$, so $a = 1$, $\theta = 0$ and M is an identity, which shows that $\Phi_2 = \tilde{\Phi}_2$. \square

3.5 Invariance under simple transformation

With the normalization mentioned above, we can get unique Beltrami signature B corresponding to domain Ω , so we can remark B as B_Ω . Now we want to prove that if we do some simple transformation like rotation, scaling and translation to Ω , the Beltrami signature is invariant.

Theorem 8. *Given a boundary simple connected domain Ω and transformation T which is composed by rotation, scaling and transformation. Let B_Ω and $B_{T(\Omega)}$ be the Beltrami signature of Ω and $T(\Omega)$, then $B_\Omega = B_{T(\Omega)}$*

Proof. Suppose $\Phi_1 : \mathbb{D} \rightarrow \Omega$, $\Phi_2 : \mathbb{D}^c \rightarrow \Omega^c$, $\tilde{\Phi}_1 : \mathbb{D} \rightarrow T(\Omega)$ and $\tilde{\Phi}_2 : \mathbb{D}^c \rightarrow T(\Omega)$ are conformal. Since T is composed by rotation, scaling and translation, T can be written as $T(z) = ke^{i\theta}z + b$. Such T is absolutely invertible and conformal.

Let $\hat{\Phi}_1 = T^{-1} \circ \tilde{\Phi}_1 : \mathbb{D} \rightarrow \Omega$, $\hat{\Phi}_1$ is conformal. Given the boundary points $\{z_1, z_2, \dots, z_n\} \subset \partial\Omega$, then $\{T(z_1), T(z_2), \dots, T(z_n)\} \subset \partial T(\Omega)$. Since $\tilde{\Phi}_1$ satisfies condition (16), we have

$$\sum_{i=1}^n \tilde{\Phi}_1^{-1}(T(z_i)) = 0.$$

Therefore

$$\sum_{i=1}^n \hat{\Phi}_1^{-1}(z_i) = \sum_{i=1}^n \tilde{\Phi}_1^{-1} \circ T(z_i) = \sum_{i=1}^n \tilde{\Phi}_1^{-1}(T(z_i)) = 0,$$

which means $\hat{\Phi}_1$ also satisfies condition (16). Hence $\hat{\Phi}_1 = T^{-1} \circ \tilde{\Phi}_1 = \Phi_1 \circ R$, which equals to

$$\hat{\Phi}_1 = T \circ \Phi_1 \circ R, \quad (22)$$

where R is a rotation.

Similarly, let $\hat{\Phi}_2 = T^{-1} \circ \tilde{\Phi}_2 : \mathbb{D}^c \rightarrow \Omega^c$, $\hat{\Phi}_2$ is conformal. Since $\tilde{\Phi}_2(\infty) = \infty$, we have

$$\hat{\Phi}_2(\infty) = T \circ \tilde{\Phi}_2(\infty) = \infty,$$

which means $\hat{\Phi}_2$ satisfies condition (19).

As for condition (20), we know that $T'(z) = ke^{i\theta}$, so

$$\hat{\Phi}'_2(z) = T' \circ \tilde{\Phi}_2(z) \cdot \tilde{\Phi}'_2(z) = ke^{i\theta} \tilde{\Phi}'_2(z). \quad (23)$$

Hence $|\hat{\Phi}'_2| = |k| |\tilde{\Phi}'_2|$, which means $\hat{\Phi}_2$ also satisfies condition (20). Therefore, $\hat{\Phi}_2 = T^{-1} \circ \tilde{\Phi}_2 = \Phi_2$ and then

$$\tilde{\Phi}_2 = T \circ \Phi_2. \quad (24)$$

We have the conformal welding

$$\tilde{f} = \tilde{\Phi}_1^{-1} \circ \tilde{\Phi}_2 = R^{-1} \circ \Phi_1^{-1} \circ T^{-1} \circ T \circ \Phi_2 = R^{-1} \circ f. \quad (25)$$

Then the harmonic extension $\tilde{F} = R^{-1} \circ F$ and

$$B_{T(\Omega)} = \mu_{\tilde{F}} = \mu_{R^{-1} \circ F} = \mu_F = B_\Omega. \quad (26)$$

□

4 Implementation detail

4.1 Zipper algorithm

In order to find an unique and stable Beltrami signature, the first thing is to do find a way to calculate a conformal mapping from the given domain to unit disk. As mentioned in Section 3.3, we only have finite boundary points of the shape and zipper algorithm invented in the 1980s is a suitable and accurate method to deal with this situation numerically.

Marshall *et al.* demonstrates the zipper algorithm detailedly with clear diagrams in [38]. For the convenience of readers, we give a very brief review here. Given N clockwise boundary points $z_1, z_2, \dots, z_N \in \partial\Omega$, this algorithm uses a series of linear fractional transformations g_1, g_2, \dots, g_N to map z_1, z_2, \dots, z_N to real axis one-by-one, and finally transform the upper half plane to unit disk by $g_{N+1}(z) = \frac{z-i}{z+i}$. Therefore, $g = g_{N+1} \circ g_N \circ \dots \circ g_2 \circ g_1$ is a conformal mapping undisputedly and maps all these boundary points to unit circle and the domain Ω to \mathbb{D} . Remark that zipper algorithm is sensitive to the order of points. If we input the points anti-clockwise, i.e. z_N, z_{N-1}, \dots, z_1 , the zipper will give us a conformal mapping from Ω^c to \mathbb{D} .

For $\Phi_1 : \mathbb{D} \rightarrow \Omega$, we can find a conformal mapping $g_{\Phi_1} : \Omega \rightarrow \mathbb{D}$ by inputting points clockwise, and $\Phi_1 = g_{\Phi_1}^{-1}$. For $\Phi_2 : \mathbb{D}^c \rightarrow \Omega^c$, we can input anti-clockwise points and get $g_{\Phi_2} : \Omega^c \rightarrow \mathbb{D}$. At the result $\Phi_2(z) = g_{\Phi_2}^{-1}(\frac{1}{z})$. Because of the invariance of scaling, the number of boundary points N is fixed as 200 here and they are picked uniformly from the shape contour.

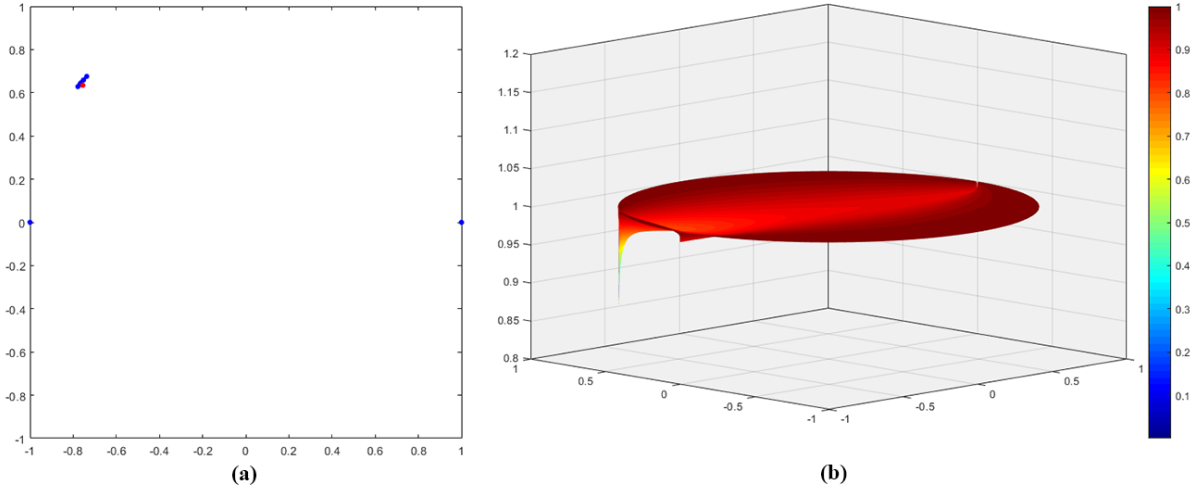


Figure 7: (a) The $p_i \in \partial\mathbb{D}$ gather in a small neighborhood around their arithmetic mean p_c , which is labeled in red. (b) The corresponding $|f(a)|$ for these p_i . It's worth to mention that the minimal of $|f(a)|$ can reach actually, but it isn't shown in the picture since the grid is not small enough.

Algorithm 1 Zipper

Inputs: $z_i \in \partial\Omega$ for $i = 1, 2, \dots, N$, $N = 200$.

Initialize: Let $r = 2$, $g_1(z) = \sqrt{\frac{z-z_2}{z-z_1}}$, $g = g_1$ and compute $p_{i,2} = g(z_i)$.

while $r < N$ **do**

 Pick $q = p_{r+1,r} = a + bi$, then compute $c = \frac{a}{|q|^2}$, $d = \frac{b}{|q|^2}$.

 Let $g_r(z) = \sqrt{\frac{cz}{1+dz}}$, then $g = g_r \circ g$ and compute $p_{i,r+1} = g_r(p_{i,r})$.

 Let $r = r + 1$.

end while

Let $g_N(z) = \left(\frac{z}{1 - \frac{z}{p_{1,N}}} \right)^2$ and $g_{N+1}(z) = \frac{z-i}{z+i}$, then $g = g_{N+1} \circ g_N \circ g$ and $p_i = g_{N+1} \circ g_N(p_{i,N})$.

return Conformal mapping $g : \Omega \rightarrow \mathbb{D}$ and boundary points $p_i \in \partial\mathbb{D}$.

4.2 Normalization

To normalize Φ_1 , we need to solve equation (18). Generally speaking, the output of zipper, $p_i = g_{\Phi_1}(z_i) \in \mathbb{D}$, $i = 1, 2, \dots, N$, will concentrate around a point. At that time, $|f(a)| \approx 1$ almost everywhere and the solution of (18) is also very close to the point. This means the solution is quite unstable and hard to converge for common algorithms (see Fig 7).

Instead of proposed a complicated method to solve equation directly, the solution we adopted to solve this problem is to use some Möbius transformations to adjust the distri-

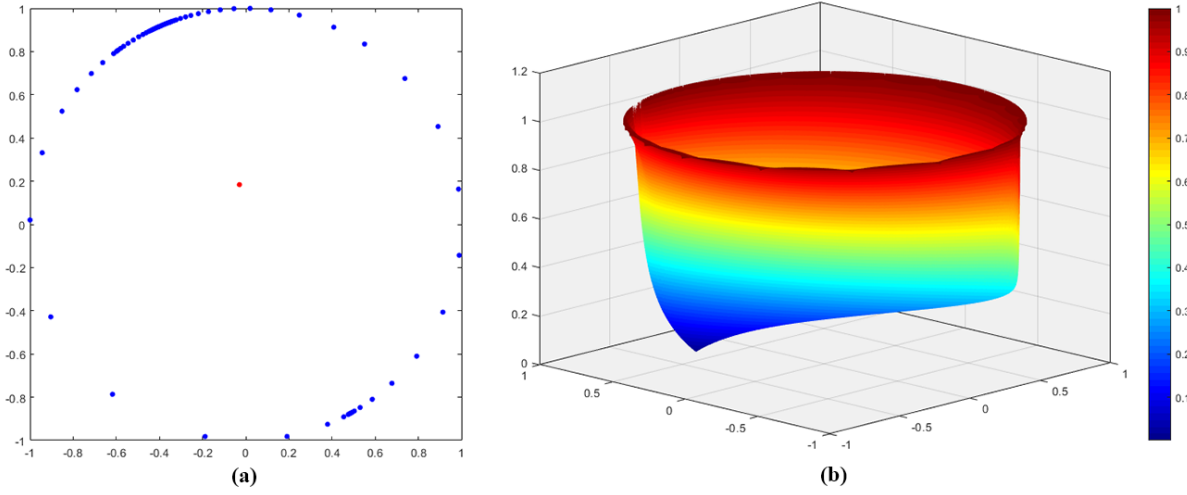


Figure 8: Similar with Fig 7. (a) The boundary points after adjustment. (b) The $|f(a)|$.

bution of p_i until it becomes almost uniform. For the r -th iteration, let

$$p_{c,r} = \frac{\sum_{i=1}^k p_{i,r}}{k} \in \mathbb{D}$$

as the arithmetic center of $p_{i,r} \in \partial\mathbb{D}$, then the Mobious transformation $M_{p_{c,r}}$ gives new boundary points on unit disk as

$$p_{i,r+1} = M_{p_{c,r}}(p_{i,r}) = \frac{p_{i,r} - p_{c,r}}{1 - \overline{p_{c,r}}p_{i,r}}.$$

Note that we set $p_{i,0} = p_i$ at the beginning. Repeat this iteration for r times until the center of boundary points is close to 0, then the distribution is sufficiently regular and Φ_1 becomes

$$\tilde{\Phi}_1 = \Phi_1 \circ M_{p_{c,0}}^{-1} \circ M_{p_{c,1}}^{-1} \circ \cdots \circ M_{p_{c,r}}^{-1}. \quad (27)$$

Now equation (18) can be solved without much effort by Newtown's method. Suppose $a \in \mathbb{D}$ is the optimal solution and the final mapping is

$$\hat{\Phi}_1 = \tilde{\Phi}_1 \circ M_a^{-1} \quad (28)$$

Algorithm 2 Normalize Φ_1

Inputs: Φ_1 and $p_i \in \partial\mathbb{D}$ for $i = 1, 2, \dots, N$, $N = 200$, $\epsilon = 0.2$.

Initialize: Let $r = 0$, $p_{i,0} = p_i$ and compute $p_{c,0} = \frac{1}{N} \sum_{i=1}^N p_i$.

while $|p_c, r| > \epsilon$ **do**

 Let $M_{p_{c,r}}(z) = \frac{z-p_{c,r}}{1-p_{c,r}z}$ and $\Phi_1 = \Phi_1 \circ M_{p_{c,r}}^{-1}$.

 Compute $p_{i,r+1} = M_{p_{c,r}}(p_{i,r})$ and $p_{c,r+1} = \frac{1}{N} \sum_{i=1}^N p_{i,r+1}$.

 Let $r = r + 1$.

end while

Solve equation (18) by Newton's method and get solution $a \in \mathbb{D}$.

Let $M_a(z) = \frac{z-a}{1-\bar{a}z}$ and $\hat{\Phi}_1 = \Phi_1 \circ M_a^{-1}$.

Compute $p_i = M_a(p_{i,r})$.

return Conformal mapping $\hat{\Phi}_1 : \mathbb{D} \rightarrow \Omega$ satisfied (16) and boundary points $p_i \in \partial\mathbb{D}$.

As for the normalization of Φ_2 , it's much easier since we only need to map ∞ to ∞ by replace Φ_2 with $\tilde{\Phi}_2(z) = \Phi_2 \circ M_b^{-1}(\frac{1}{z})$, where $b = \Phi_2^{-1}(\infty)$. Another requirement (20) can be satisfied by finding $a = \arg \max_{z \in \partial\mathbb{D}} |\tilde{\Phi}'_2(z)|$. Since we know each linear fractional transformation composing Φ_2 , the derivative of $\tilde{\Phi}_2$ can be found by the chain derivative rule. Here we select 10^5 points from $[0, 2\pi)$ as θ_j and calculate the $|\tilde{\Phi}'_2(e^{i\theta_j})|$ (see Fig 10).

Therefore, the maximal solution $\theta_{\max} = \arg \max_{j \in [1, 10^5]} |\tilde{\Phi}'_2(e^{i\theta_j})|$ can be used to normalize the rotation and the final mapping is

$$\hat{\Phi}_2(z) = \tilde{\Phi}_2(e^{i\theta_{\max}} z). \quad (29)$$

This grid can generate a triangluar mesh M and we will calculate the Beltrami coefficient on M .

Algorithm 3 Normalize Φ_2

Inputs: Φ_2 and $p_i \in \partial\mathbb{D}$ for $i = 1, 2, \dots, N$, $N = 200$, $M = 10^5$.

Compute $b = \Phi_2^{-1}(\infty)$.

Let $M_b(z) = \frac{z-b}{1-\bar{b}z}$ and $\tilde{\Phi}_2(z) = \Phi_2 \circ M_b^{-1}(\frac{1}{z})$.

Calculate $|\tilde{\Phi}'_2|$ by chain derative rule.

Let $\theta_j = \frac{2\pi}{M}(j-1)$ for $j = 1, 2, \dots, M$.

Compute $|\tilde{\Phi}'_2| (e^{i\theta_j})$.

Find maximal value and corresponding θ_{\max} .

Let $\hat{\Phi}_2(z) = \tilde{\Phi}_2(e^{i\theta_{\max}} z)$ and compute $p_i = \frac{e^{-i\theta_{\max}}}{M_b(p_i)}$.

return Conformal mapping $\Phi_1 : \mathbb{D}^c \rightarrow \Omega^c$ satisfied (19), (20) and boundary points $p_i \in \partial\mathbb{D}$.

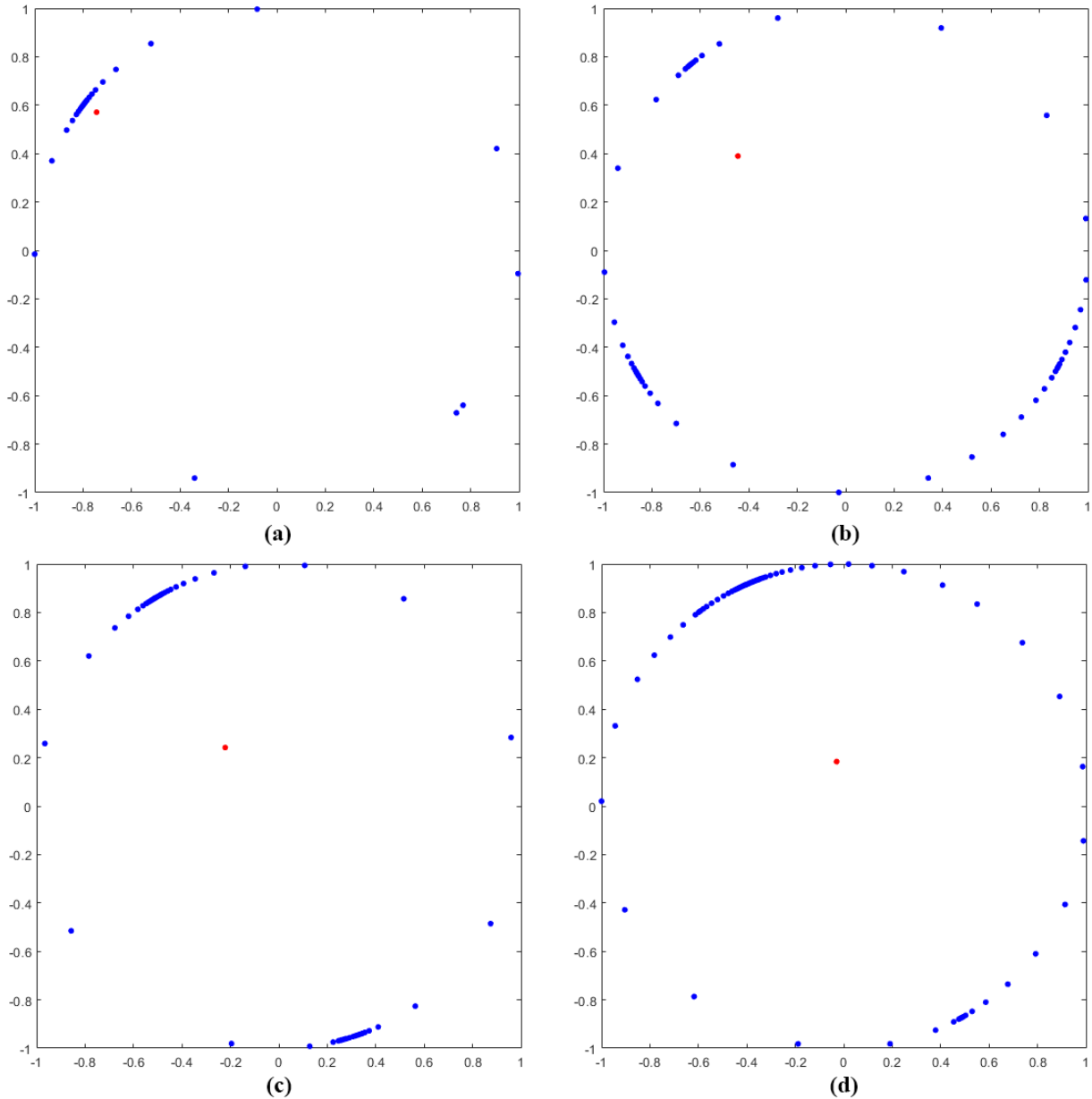


Figure 9: The iteration of distribution adjustment. The boundary points are blue and their arithmetic center is red in each picture. (a)-(d) The 1st, 3rd, 7th, 12th iteration.

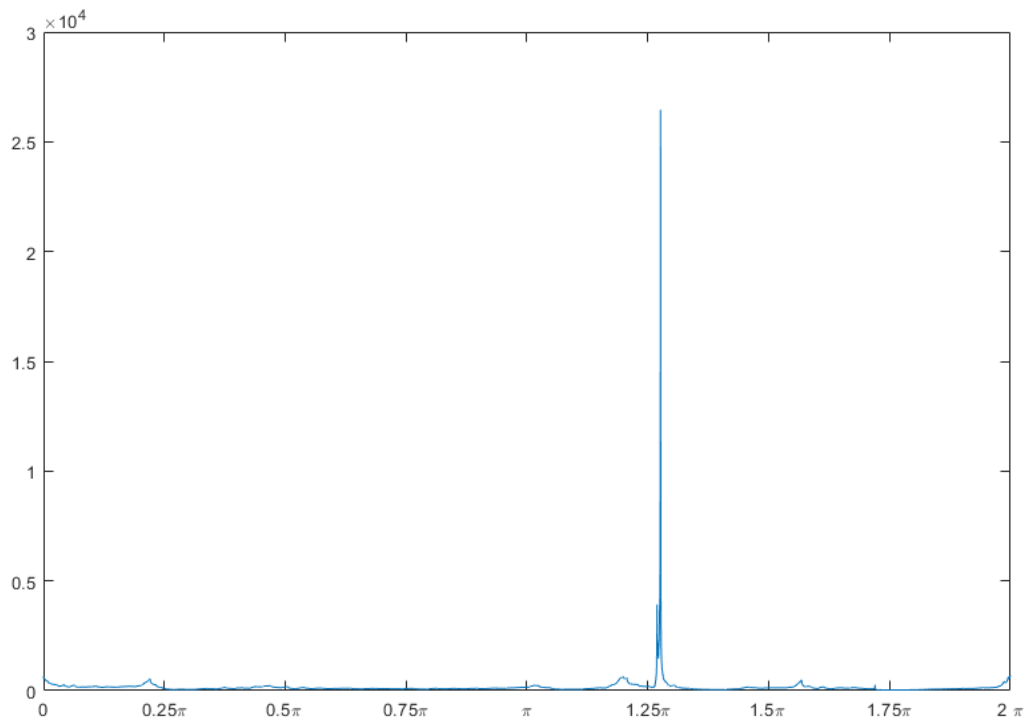


Figure 10: The change of $|\tilde{\Phi}'_2(e^{i\theta_j})|$ for different $\theta_j \in [0, 2\pi)$. It shows this function has a significant maximum and θ_{max} is about 1.25π .

4.3 Harmonic extension

After obtaining the normalized $\hat{\Phi}_1$ and $\hat{\Phi}_2$, the conformal welding can be represented as a series points $(\varphi_i, \omega_i) = (\arg(\hat{\Phi}_2^{-1}(z_i)), \arg(\hat{\Phi}_1^{-1}(z_i)))$, where $\varphi_i, \omega_i \in [0, 2\pi)$. So in fact we should use discrete form Poisson integral to extend f to a harmonic mapping F on the unit disk.

$$F(re^{i\theta}) = \frac{1}{2\pi} \sum_{j=1}^k \frac{(1-r^2)e^{i\omega_j}}{1-2r\cos(\varphi_j - \theta) + r^2} ((\varphi_j - \varphi_{j-1}) \bmod 2\pi), \quad (30)$$

where $\varphi_0 = \varphi_k$ and this mod can solve some critical value problem, for example, $\varphi_j = 0$ but $\varphi_{j-1} = 6$. For the convenience of computation, we only calculate the value of F on a grid

$$G = \{z = x + iy \mid |z| \leq 1, x = \frac{j}{100}, y = \frac{k}{100}, j, k = -100, -99, \dots, 99, 100\}. \quad (31)$$

4.4 Summary of the Algorithm

The totally algorithm is as following.

Algorithm 4 Calculate Beltrami signature

Inputs: Bounded simple connected shape $\Omega \subset \mathbb{C}$, $N = 200$.

Pick N clockwise points z_1, z_2, \dots, z_N from $\partial\Omega$ uniformly.

Input z_1, z_2, \dots, z_N to Algorithm 1 and get conformal mapping $g_{\Phi_1} : \mathbb{D} \rightarrow \Omega$ and $p_{i,1} \in \partial\mathbb{D}$.

Let $\Phi_1(z) = g_{\Phi_1}^{-1}(z)$ and input it and $p_{i,1}$ to Algorithm 2, then get normalized $\hat{\Phi}_1$ and $p_{i,1}$.
Input z_N, \dots, z_2, z_1 to Algorithm 1 and get conformal mapping $g_{\Phi_2} : \mathbb{D} \rightarrow \Omega^c$ and $p_{i,2} \in \partial\mathbb{D}$.

Let $\Phi_2(z) = g_{\Phi_2}^{-1}(\frac{1}{z})$ and input it and $p_{i,2}$ to Algorithm 3, then get normalized $\hat{\Phi}_2$ and $p_{i,2}$.

Let $f = \hat{\Phi}_1^{-1} \circ \hat{\Phi}_2$ and represent it by $(\varphi_i, \omega_i) = (\arg(p_{i,2}), \arg(p_{i,1}))$.

Extend f to F on \mathbb{D} by equation (30) on grid G .

Calculate Beltrami coefficient B of F on M .

return Beltrami signature B .

5 Experimental result

In this section, we will validate key properties of our proposed Beltrami signature, the invariance of under simple transformations and the robustness under small distortion and modification. Besides that, a good shape representation should keep the similarity with the same kind shape and is significantly different from different kinds of shape.

Before showing results, what needs illustration is that the distance we used to measure the difference of Beltrami signature is based on L^2 norm,

$$d(B_1, B_2) = \sqrt{\frac{1}{N} \sum_{i=1}^N |B_1(z_i) - B_2(z_i)|^2}, \quad (32)$$

where B_1, B_2 are two different Beltrami signature, $z_i \in \mathbb{D}$ is the face center of triangular mesh M mentioned in Section 4.3 and $N = 60962$ here.

5.1 Invariance

We use the dolphin shown in Fig 5 (a) as the original shape, then calculate Beltrami signature after scaling, translation and rotation and compare them with the original shape's Beltrami signature. The result is displayed in Fig 11. In this figure, the first column are the sets of boundary points and we remark them as Ω_a to Ω_f . The second column are the corresponding Beltrami signatures B_a to B_f . Note that all the Beltrami signatures are shown in modulus, i.e. $|B_n|$ for row n , and in top view. And the third column(if have) are the histograms of the difference between original shape's Beltrami signature, i.e. $|B_n - B_a|$ for row n .

Row b and c are about scaling, the shapes are $\Omega_b = \{z \mid z = 1.5z_a, z_a \in \Omega_a\}$ and $\Omega_c = \{z \mid z = 0.5z_a, z_a \in \Omega_a\}$ and the distance are $d(B_a, B_b) = 5.5647 \times 10^{-8}$ and $d(B_a, B_c) = 5.3476 \times 10^{-8}$. Row d is about translation, the shape $\Omega_d = \{z \mid z = z_a + 100 + 20i, z_a \in \Omega_a\}$ and the distance is $d(B_a, B_d) = 4.7817 \times 10^{-8}$. Row e is about rotation, the shape is $\Omega_e = \{z \mid z = e^{0.2\pi i} z_a, z_a \in \Omega_a\}$ and the distance is $d(B_a, B_e) = 5.2144 \times 10^{-8}$. Row f is the combination of scaling, translation and rotation, the shape is $\Omega_f = \{z \mid z = 3e^{-0.85\pi i} z_a + 350 + 600i, z_a \in \Omega_a\}$ and the distance is $d(B_a, B_f) = 5.7635 \times 10^{-8}$. These confirm the invariance of Beltrami signature and scaling, translation and rotation.

5.2 Robustness

Similar with Section 5.1, here we still treat the dolphin as the original shape and modify some small parts of it and Fig 12 is the result. It shows that the proposed signature is robust and stable and will not have a big mutation caused by small disturbance.

Row g, h and i are result about modification. These shapes are generated by removing or adding something, which is in the red circle. We can see that Beltrami signatures have slight differences from B_a but are still similar in general. And this figure also demonstrates that the bigger the modification part is, the more different the Beltrami signature is. For example in row i, losing a half of the tail makes the signature has a marked change. Quantitatively, $d(B_a, B_g) = 0.0132$, $d(B_a, B_h) = 0.0316$ and $d(B_a, B_i) = 0.1761$.

Row j is for distortion. This dolphin is only enlarged in horizontally and becomes fatter, then the B_j moves a little bit and $d(B_a, B_j) = 0.0724$.

5.3 Classification with Beltrami signature

Above properties ensure the proposed signature having the ability to reflect some stable features of given shape, but another much more important thing people concerned is that whether it can distinguish a shape from many different kinds of shapes and classify it correctly.

To compare the classification performance, we also use conformal welding directly to

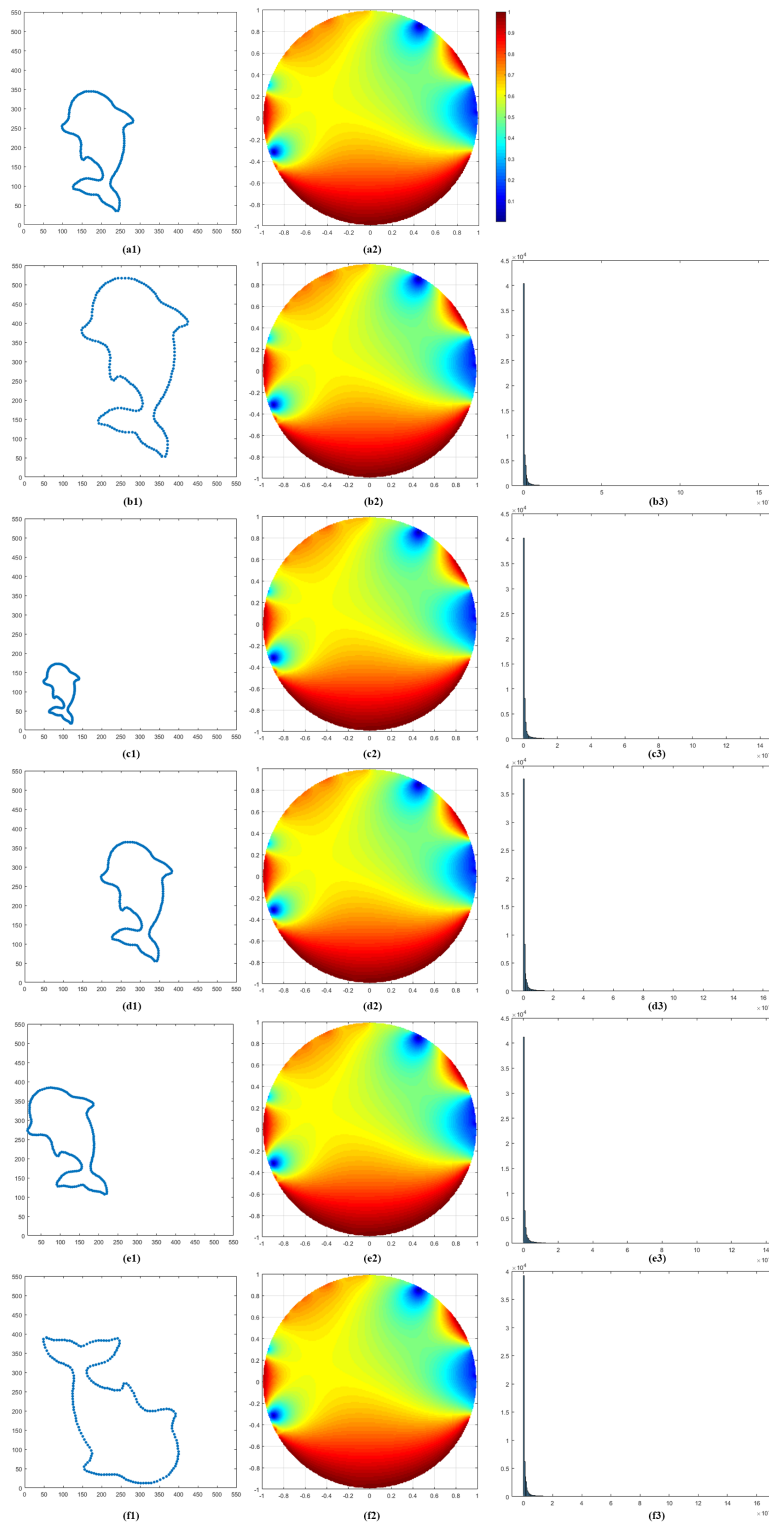


Figure 11: Beltrami signature under scaling, translation and rotation.

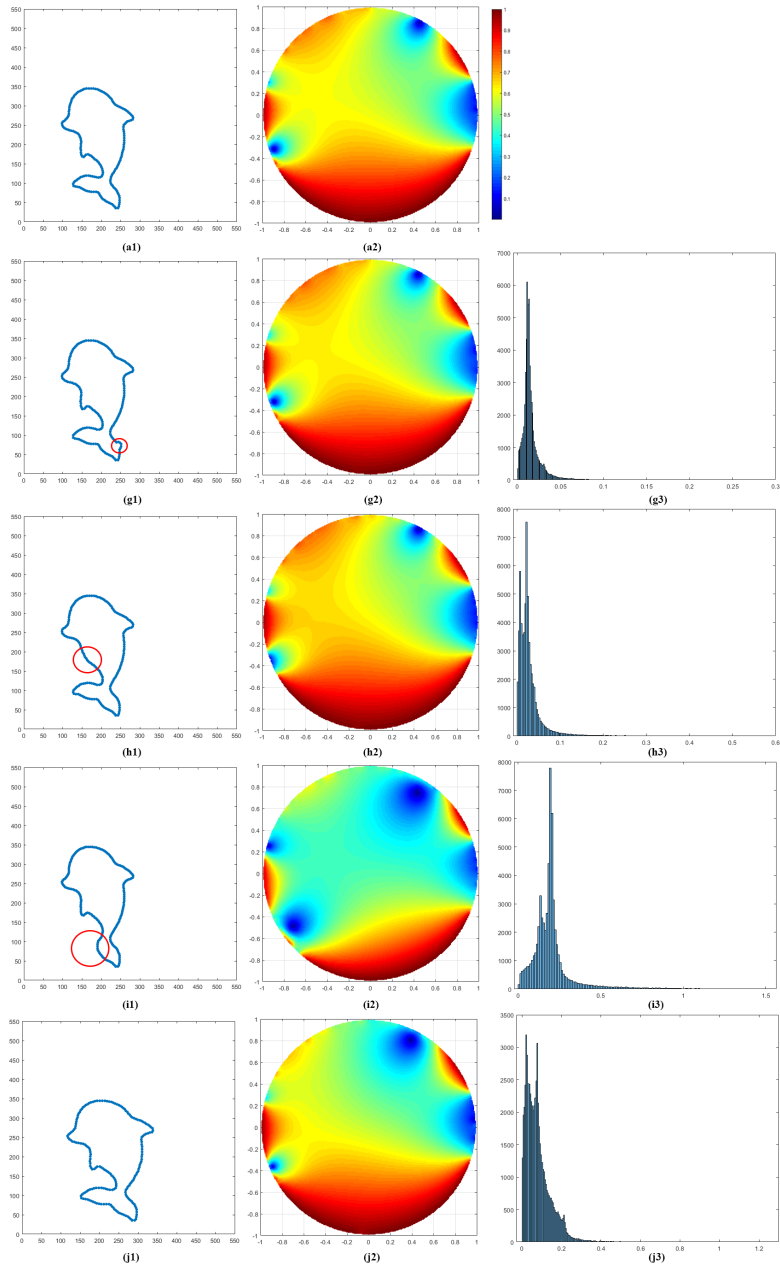


Figure 12: Beltrami signature under small modification

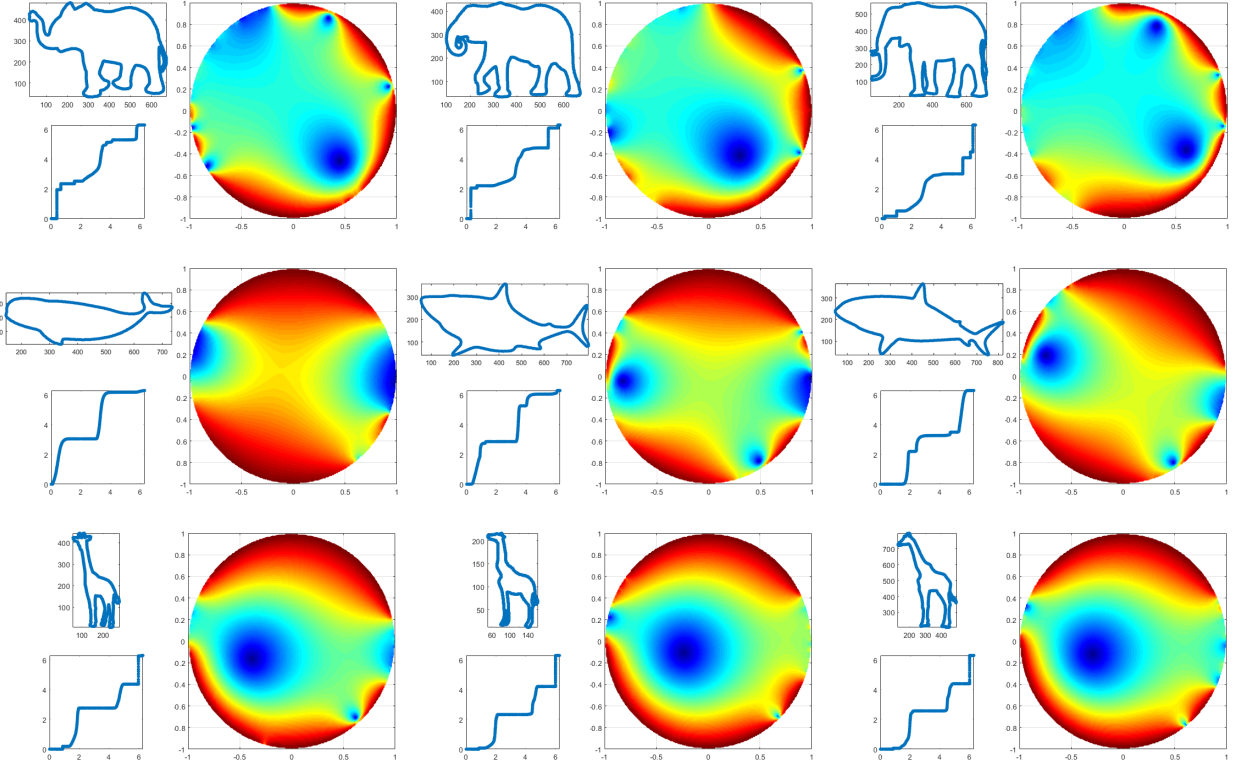


Figure 13: These 3 rows are elephant, fish and giraffe. In each subfigure, the top left is the input shape, bottom left is the conformal welding and the right is Beltrami signature.

classify, and the distance is defined as

$$d_c(f_1, f_2) = \sqrt{\frac{1}{N} \sum_{i=1}^N |f_1(z_i) - f_2(z_i)|^2}, \quad (33)$$

where f_1, f_2 are two different conformal welding, $N = 200$ here.

We prepare 3 kinds of animals, fish, giraffe and elephant. There are 3 images for each group so 9 images in total. From Fig 13, we can find that each class share similar Beltrami signatures and conformal welding. From Fig 14, the inter-class distance of Beltrami signature is awlays less than 0.2 while the intra-class distance is greater than 0.2. But for conformal welding, the data is messy, for example, fish 3 thinks itself is very different from other fishes but looks most like giraffe 2. After multidimensional scaling(MDS), we can maps all these 9 shapes to points on 2D plane as Fig 15, where the Beltrami signature shows powerful classification ablity.

5.4 Classification for more classes

In this experiment, we enlarge the amount of images to 58 in 7 different classes, camel, deer, dog, elephant, giraffe, gorilla and rabbit. We calculate the distance matrix by equation

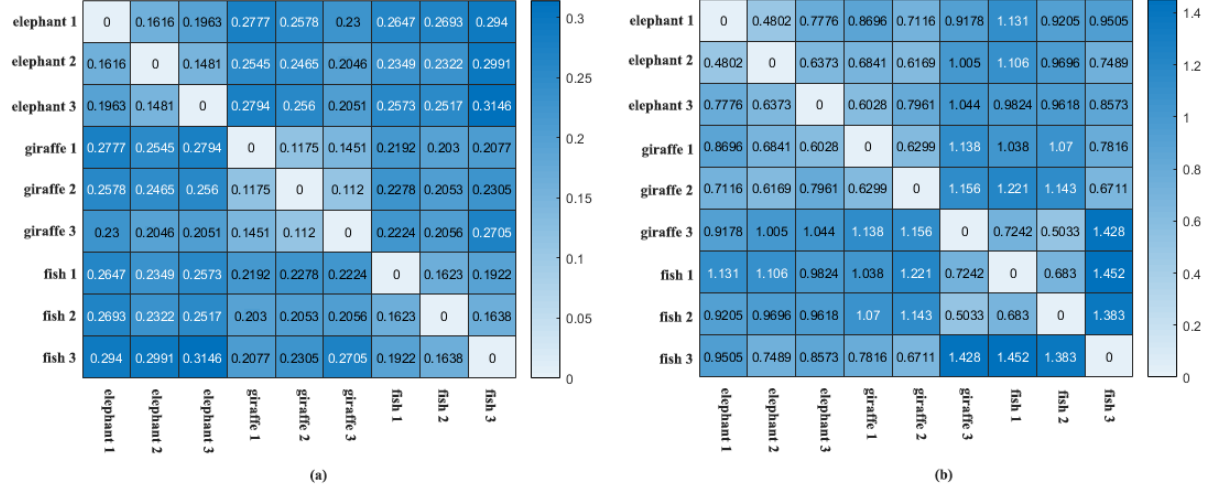


Figure 14: (a) The distance matrix of Beltrami signatures of above 9 shapes by equation (32). (b) The distance matrix of conformal weldings by equation (33).

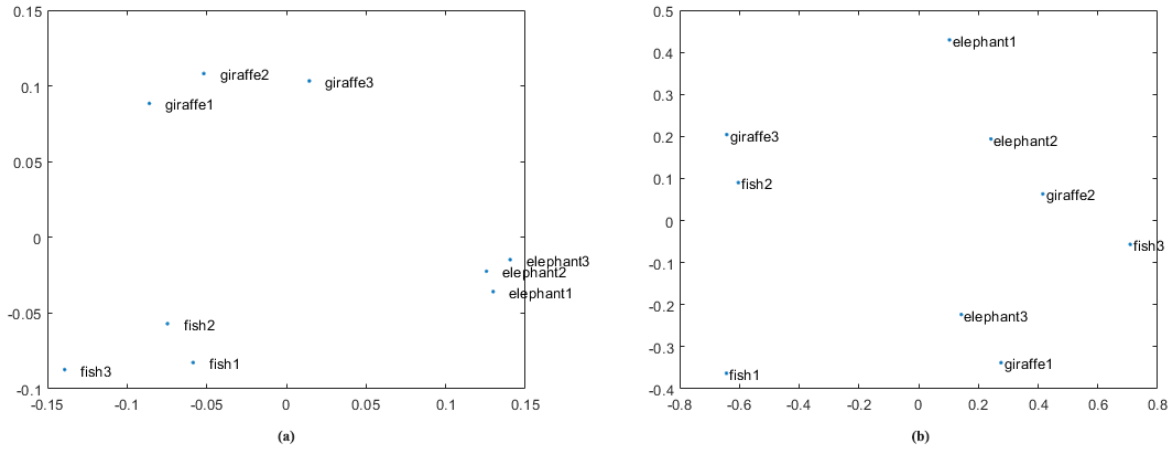


Figure 15: (a) The MDS result of Beltrami signature. (b) The MDS result of conformal welding.

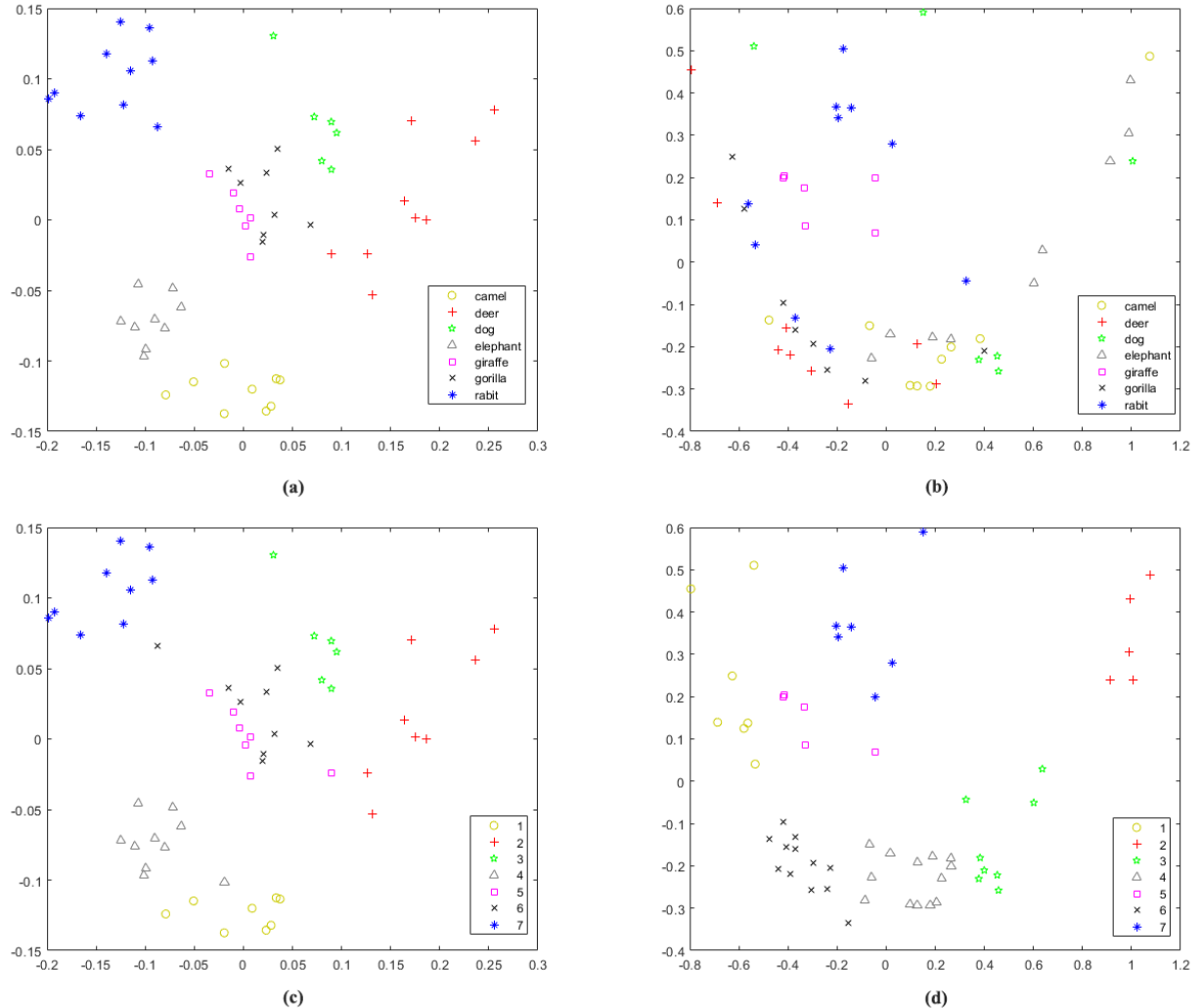


Figure 16: (a) The MDS result of Beltrami signature. (b) The MDS result of conformal welding. (c) The clustering result of Beltrami signature. (d) The clustering results of conformal welding.

(32) and (33) and use MDS to remap these shapes to 2D plane accordingly, then k -medoids method is used to cluster these points to 7 classes. The MDS and clustering results based on Beltrami signature and conformal welding are displayed in Fig 16. The classification accuracy based on Beltrami signature is 94.83%, while the accuracy based on conformal welding is only 37.93%.

6 Conclusion

In this paper, we propose a novel shape representation for 2D bounded simple connected objects called Beltrami signature. The proposed signature is based on conformal welding but overcome a key shortcoming that it can be uniquely determined by the given shape. What's more exciting is that the proposed representation is invariance under scaling, translation and rotation. For slight deformation and distortion, Beltrami signature keeps roubost and only changes within a reasonable small range. Therefore, there are reasons to believe the it does have ablity to represent some invariant geometrical features. The experimental results also confirm that the Beltrami signature has excellent performance in multi-classification tasks.

Although our work has achieved relatively good results, the proposed representation still have some limitations. Firstly, the Beltrami signature is only applicable to simple connected shapes currently, but as a matter of fact, multi connected images are the majority in the real world. So we are eager for a feasible method to extend our Beltrami signature to multi connected situation. Secondly, the traditional algorithm to compute the Beltrami coefficient is inevitably dependent on triangluar mesh, which consumes a lot of time. Therefore, a fast algorithm to obatin this signature avoiding dense mesh is of high priority in our future work. Thirdly, when normalizing the conformal mapping Φ_2 from exterior of unit disk to exterior of the domain, the position where the derivation of Φ_2 reaches the maximum value is used to adjust the rotation. We trust this point in the original image has a certain geometric meaning, whereas it is not clear at present.

In summary, we will focus on third marjor directions in the future. One is that the deeper meaning of Beltrami signature is worth digging and then a multi-connected version of representation based on this work can be proposed. Another is that if the Beltrami signature contains some geometrical features of shapes, we can also extract them directly from images and generate the Beltrami signature again. Hence the deep learning theory may help us to compute this signature from given images immediately, which is very likely to improve algorithm speed performance greatly. A third direction is this representation can be used in more applications like segementation, registration and so on.

References

- [1] S. Belongie, J. Malik, and J. Puzicha, “Shape matching and object recognition using shape contexts,” *IEEE transactions on pattern analysis and machine intelligence*, vol. 24, no. 4, pp. 509–522, 2002.

- [2] G. G. Demisse, D. Aouada, and B. Ottersten, “Deformation based curved shape representation,” *IEEE transactions on pattern analysis and machine intelligence*, vol. 40, no. 6, pp. 1338–1351, 2017.
- [3] M. Hagedoorn, “Pattern matching using similarity measures,” Ph.D. dissertation, Universiteit Utrecht, 2000.
- [4] M. Lades, J. C. Vorbruggen, J. Buhmann, J. Lange, C. Von Der Malsburg, R. P. Wurtz, and W. Konen, “Distortion invariant object recognition in the dynamic link architecture,” *IEEE Transactions on computers*, vol. 42, no. 3, pp. 300–311, 1993.
- [5] L. J. Latecki, R. Lakamper, and T. Eckhardt, “Shape descriptors for non-rigid shapes with a single closed contour,” in *Proceedings IEEE Conference on Computer Vision and Pattern Recognition. CVPR 2000 (Cat. No. PR00662)*, vol. 1. IEEE, 2000, pp. 424–429.
- [6] F. Mokhtarian, S. Abbasi, and J. Kittler, “Efficient and robust retrieval by shape content through curvature scale space,” in *Image Databases and Multi-Media Search*. World Scientific, 1997, pp. 51–58.
- [7] C. T. Zahn and R. Z. Roskies, “Fourier descriptors for plane closed curves,” *IEEE Transactions on computers*, vol. 100, no. 3, pp. 269–281, 1972.
- [8] E. Sharon and D. Mumford, “2d-shape analysis using conformal mapping,” *International Journal of Computer Vision*, vol. 70, no. 1, pp. 55–75, 2006.
- [9] O. McEnteggart, J. Miller, and W. Qian, “Uniqueness of the welding problem for sl and liouville quantum gravity,” *arXiv preprint arXiv:1809.02092*, 2018.
- [10] Y. Katznelson, S. Nag, and D. Sullivan, “On conformal welding homeomorphisms associated to jordan curves,” *Ann. Acad. Sci. Fenn. Ser. AI Math*, vol. 15, no. 2, pp. 293–306, 1990.
- [11] D. E. Marshall, “Conformal welding for finitely connected regions,” *Computational Methods and Function Theory*, vol. 11, no. 2, pp. 655–669, 2012.
- [12] L. M. Lui, W. Zeng, S.-T. Yau, and X. Gu, “Shape analysis of planar multiply-connected objects using conformal welding,” *IEEE transactions on pattern analysis and machine intelligence*, vol. 36, no. 7, pp. 1384–1401, 2013.
- [13] K. Astala, P. Jones, A. Kupiainen, and E. Saksman, “Random curves by conformal welding,” *Comptes Rendus Mathematique*, vol. 348, no. 5-6, pp. 257–262, 2010.
- [14] C. Y. Siu, H. L. Chan, and R. L. Ming Lui, “Image segmentation with partial convexity shape prior using discrete conformality structures,” *SIAM Journal on Imaging Sciences*, vol. 13, no. 4, pp. 2105–2139, 2020.
- [15] H.-L. Chan, S. Yan, L.-M. Lui, and X.-C. Tai, “Topology-preserving image segmentation by beltrami representation of shapes,” *Journal of Mathematical Imaging and Vision*, vol. 60, no. 3, pp. 401–421, 2018.

- [16] D. Zhang and L. M. Lui, “Topology-preserving 3d image segmentation based on hyper-elastic regularization,” *Journal of Scientific Computing*, 2020, accepted.
- [17] K. C. Lam and L. M. Lui, “Landmark-and intensity-based registration with large deformations via quasi-conformal maps,” *SIAM Journal on Imaging Sciences*, vol. 7, no. 4, pp. 2364–2392, 2014.
- [18] L. M. Lui, K. C. Lam, S.-T. Yau, and X. Gu, “Teichmuller mapping (t-map) and its applications to landmark matching registration,” *SIAM Journal on Imaging Sciences*, vol. 7, no. 1, pp. 391–426, 2014.
- [19] T. C. Ng, X. Gu, and L. M. Lui, “Computing extremal teichmüller map of multiply-connected domains via beltrami holomorphic flow,” *Journal of Scientific Computing*, vol. 60, no. 2, pp. 249–275, 2014.
- [20] L. M. Lui, T. W. Wong, W. Zeng, X. Gu, P. M. Thompson, T. F. Chan, and S.-T. Yau, “Optimization of surface registrations using beltrami holomorphic flow,” *Journal of scientific computing*, vol. 50, no. 3, pp. 557–585, 2012.
- [21] K. C. Lam, X. Gu, and L. M. Lui, “Genus-one surface registration via teichmüller extremal mapping,” in *International Conference on Medical Image Computing and Computer-Assisted Intervention*. Springer, 2014, pp. 25–32.
- [22] M. Zhang, F. Li, Y. He, S. Lin, D. Wang, and L. M. Lui, “Registration of brainstem surfaces in adolescent idiopathic scoliosis using discrete ricci flow,” in *International Conference on Medical Image Computing and Computer-Assisted Intervention*. Springer, 2012, pp. 146–154.
- [23] Y. T. Lee, K. C. Lam, and L. M. Lui, “Landmark-matching transformation with large deformation via n-dimensional quasi-conformal maps,” *Journal of Scientific Computing*, vol. 67, no. 3, pp. 926–954, 2016.
- [24] L. M. Lui, S. Thiruvenkadam, Y. Wang, P. M. Thompson, and T. F. Chan, “Optimized conformal surface registration with shape-based landmark matching,” *SIAM Journal on Imaging Sciences*, vol. 3, no. 1, pp. 52–78, 2010.
- [25] L. M. Lui, K. C. Lam, T. W. Wong, and X. Gu, “Texture map and video compression using beltrami representation,” *SIAM Journal on Imaging Sciences*, vol. 6, no. 4, pp. 1880–1902, 2013.
- [26] L. M. Lui, T. W. Wong, P. Thompson, T. Chan, X. Gu, and S.-T. Yau, “Shape-based diffeomorphic registration on hippocampal surfaces using beltrami holomorphic flow,” in *International Conference on Medical Image Computing and Computer-Assisted Intervention*. Springer, 2010, pp. 323–330.
- [27] L. M. Lui, S. Thiruvenkadam, Y. Wang, P. M. Thompson, and T. F. Chan, “Optimized conformal surface registration with shape-based landmark matching,” *SIAM Journal on Imaging Sciences*, vol. 3, no. 1, pp. 52–78, 2010.

- [28] L. M. Lui and C. Wen, “Geometric registration of high-genus surfaces,” *SIAM Journal on Imaging Sciences*, vol. 7, no. 1, pp. 337–365, 2014.
- [29] P. T. Choi, K. C. Lam, and L. M. Lui, “Flash: Fast landmark aligned spherical harmonic parameterization for genus-0 closed brain surfaces,” *SIAM Journal on Imaging Sciences*, vol. 8, no. 1, pp. 67–94, 2015.
- [30] Y. Wang, L. M. Lui, X. Gu, K. M. Hayashi, T. F. Chan, A. W. Toga, P. M. Thompson, and S.-T. Yau, “Brain surface conformal parameterization using riemann surface structure,” *IEEE transactions on medical imaging*, vol. 26, no. 6, pp. 853–865, 2007.
- [31] L. M. Lui, Y. Wang, T. F. Chan, and P. Thompson, “Landmark constrained genus zero surface conformal mapping and its application to brain mapping research,” *Applied Numerical Mathematics*, vol. 57, no. 5-7, pp. 847–858, 2007.
- [32] G. P. Choi, D. Qiu, and L. M. Lui, “Shape analysis via inconsistent surface registration,” *Proceedings of the Royal Society A*, vol. 476, no. 2242, p. 20200147, 2020.
- [33] H. L. Chan, H. Li, and L. M. Lui, “Quasi-conformal statistical shape analysis of hippocampal surfaces for alzheimer’s disease analysis,” *Neurocomputing*, vol. 175, pp. 177–187, 2016.
- [34] W. Zeng, L. M. Lui, X. Gu, S.-T. Yau *et al.*, “Shape analysis by conformal modules,” *Methods and Applications of Analysis*, vol. 15, no. 4, pp. 539–556, 2008.
- [35] L. M. Lui, W. Zeng, S.-T. Yau, and X. Gu, “Shape analysis of planar multiply-connected objects using conformal welding,” *IEEE transactions on pattern analysis and machine intelligence*, vol. 36, no. 7, pp. 1384–1401, 2013.
- [36] ——, “Shape analysis of planar objects with arbitrary topologies using conformal geometry,” in *European Conference on Computer Vision*. Springer, 2010, pp. 672–686.
- [37] S. Chen, S. Ponnusamy, X. Wang *et al.*, “Compositions of harmonic mappings and biharmonic mappings,” *Bulletin of the Belgian Mathematical Society-Simon Stevin*, vol. 17, no. 4, pp. 693–704, 2010.
- [38] D. E. Marshall and S. Rohde, “Convergence of a variant of the zipper algorithm for conformal mapping,” *SIAM Journal on Numerical Analysis*, vol. 45, no. 6, pp. 2577–2609, 2007.